Dynamic heterogeneity in active glass-forming liquids is qualitatively different compared to its equilibrium behaviour: Supplementary Materials

Kallol Paul[1], Saroj Kumar Nandi[1], and Smarajit Karmakar[1*]
[1] *TIFR Center for Interdisciplinary Science, Tata Institute of Fundamental Research, 36/P Gopanpally Village, Serilingampally Mandal, RR District, Hyderabad, 500075, Telangana, India*

[*] smarajit@tifrh.res.in

I. MODEL AND METHODS

The models studied are generic glass-forming liquids in three dimensions (3D). One is a Kob-Andersen binary mixture whose amount of bi-dispersity was chosen to avoid crystallization as well as phase separation. In this article we refer it as **3dKA model**. A particle of type α and a particle of type β ($\alpha\beta = \mathrm{AA}, \mathrm{AB}, \mathrm{BB}$), separated by a distance r from each other, interact via a Lenard-Jones potential given by

$$\Phi_{\alpha\beta}(r) = \begin{cases} 4\varepsilon_{\alpha\beta}\left[\left(\frac{\sigma_{\alpha\beta}}{r}\right)^{12} - \left(\frac{\sigma_{\alpha\beta}}{r}\right)^{6}\right], & \text{if } r \leq r_{\mathrm{c}}\sigma_{\alpha\beta} \\ 0, \qquad \text{if } r \geq r_{\mathrm{c}}\sigma_{\alpha\beta}, \end{cases} \tag{1}$$

where r_{c} is the cut-off length above which the potential vanishes. In this work, energies and lengths are given in units of $\varepsilon_{\mathrm{AA}}$ and σ_{AA}, respectively. The parameters of the potential are $\varepsilon_{\mathrm{AB}} = 1.5\varepsilon_{\mathrm{AA}}$, $\varepsilon_{\mathrm{BB}} = 0.5\varepsilon_{\mathrm{AA}}$, $\sigma_{\mathrm{AB}} = 0.8\sigma_{\mathrm{AA}}$, and $\sigma_{\mathrm{BB}} = 0.88\sigma_{\mathrm{AA}}$. The Boltzmann constant as well as mass of the particles are set to unity, $k_{\mathrm{B}} = 1.0$ and $m = 1.0$, respectively. Moreover, we set $r_{\mathrm{c}} = 2.5$. The number density is chosen to be $\rho = N/V = 1.2$ (with N the particle number and V the volume of the system). The number of particles N is 50000 and the bi-dispersity ratio was $80:20$ $(A:B)$.

To test the generic nature of our results, we chose another model, with Harmonic interaction between a pair of particles, that interpolates between finite-temperature glasses and hard-sphere glasses. This model has been studied extensively in the context of jamming physics. In this article we refer it as **3dHP model**. This is a $50:50$ binary mixture with diameter ratio of 1.4. The interaction potential is given by

$$\Phi\left(\frac{r_{ij}}{\sigma_{ij}}\right) = \epsilon\left[1 - \left(\frac{r_{ij}}{\sigma_{ij}}\right)^{2}\right], \tag{2}$$

for $r_{ij} < \sigma_{ij}$ and 0 otherwise. Considering the diameters of ith and jth particles as σ_i and σ_j, we define $\sigma_{ij} = (\sigma_i + \sigma_j)/2$. We simulated this model at a constant density $\rho = 0.82$ and temperature, T, as a control parameter. The value of ϵ is chosen to be 4.0.

We have done NVT simulations and the equations of motion are integrated with velocity-Verlet integration scheme using an integration time step of $\delta t = 0.005\,\tau$ with $\tau = \sqrt{m\sigma_{\mathrm{AA}}^2/\varepsilon_{\mathrm{AA}}}$. For all the simulations we have first equilibrated our systems at least for $50\tau_\alpha$ and stored data for similar simulation time. To keep the temperature constant we used Gaussian operator-splitting thermostat throughout our simulation [1]. We have also performed 20 statistically independent simulations for each T and system size studied for better averaging. Note that usual Berendsen thermostat does not do a good job of maintaining the T in this non-equilibrium simulations in presence of active forcing, but the Gaussian operator splitting thermostat is found to maintain the system at the desired T without any deviation.

We introduced activity for a fraction ρ_a of the total number of particles in the system. These active particles are chosen randomly and assigned a self-propulsion forces of the form $\vec{f} = f_0(k_x\hat{x} + k_y\hat{y} + k_z\hat{z})$ where k_x, k_y, k_z are ± 1, chosen randomly to maintain the momentum conservation up to a persistence time τ_p. After the persistence time τ_p the set of values of k_x, k_y, k_z are changed maintaining the momentum conservation. In this work, we keep $\rho_a = 0.1$ and $\tau_p = 1.0$ fixed and study the effect of activity as a function of f_0 only.

II. COMPUTING DYNAMIC HETEROGENEITY LENGTH SCALE

We have used three different techniques to compute the dynamic heterogeneity length scale ξ_D for all studied activities.

A. Block analysis of χ_4^P

As the time scale is gradually decreasing with increasing activity at a constant T we chose a temperature window for each f_0 such that we can have a similar τ_α range for all activity. We performed the MD simulations at those temperatures for each f_0. To extract the dynamic length scale, ξ_D, of the system at all studied activity values, we used a newly proposed method "block analysis", an efficient method to perform finite-size scaling for obtaining the length scale of dynamic heterogeneity [2]. This method involves considering a small sub-system (referred here as blocks) of varying sizes embedded in a system of a fixed (large) size. The length scale associated with dynamic heterogeneity is obtained from a finite-size scaling analysis of the dependence of the four-point dynamic susceptibility, $\chi_4(t)$ (see definition later) on the block size. All the simulations are carried out for a single, moderately large system

size, $N = 50000$. We then construct blocks of size $L_B = L/n$, where $n \in \{3, 4, 5, ...\}$ and calculate various dynamic quantities using the particles which are present inside one such box at a chosen time origin. Then we compute the self overlap correlation function, $Q(L_B, t)$, for a particular block size,

$$Q(L_B, t) = \frac{1}{N_B} \sum_{i=1}^{N_B} \frac{1}{n_i} \sum_{j=1}^{n_i} \langle w(|\, \mathbf{r}_j(t) - \mathbf{r}_j(0)\, |) \rangle \,, \tag{3}$$

where N_B is the number of blocks with size L_B, n_i is the number of particles in the ith block at time $t = 0$, and the window function $w(x) = \Theta(a - x)$ where Θ is the Heaviside step function and the value of the parameter a is chosen to remove the de-correlation arising from vibrations of particles inside the cages formed by their neighbours. The dynamical susceptibility associated with blocks of size L_B is then defined as follows

$$\chi_4(L_B, t) = \frac{N L_B^3}{L_0^3} \left\langle [Q(L_B, t) - \langle Q(L_B, t) \rangle]^2 \right\rangle \tag{4}$$

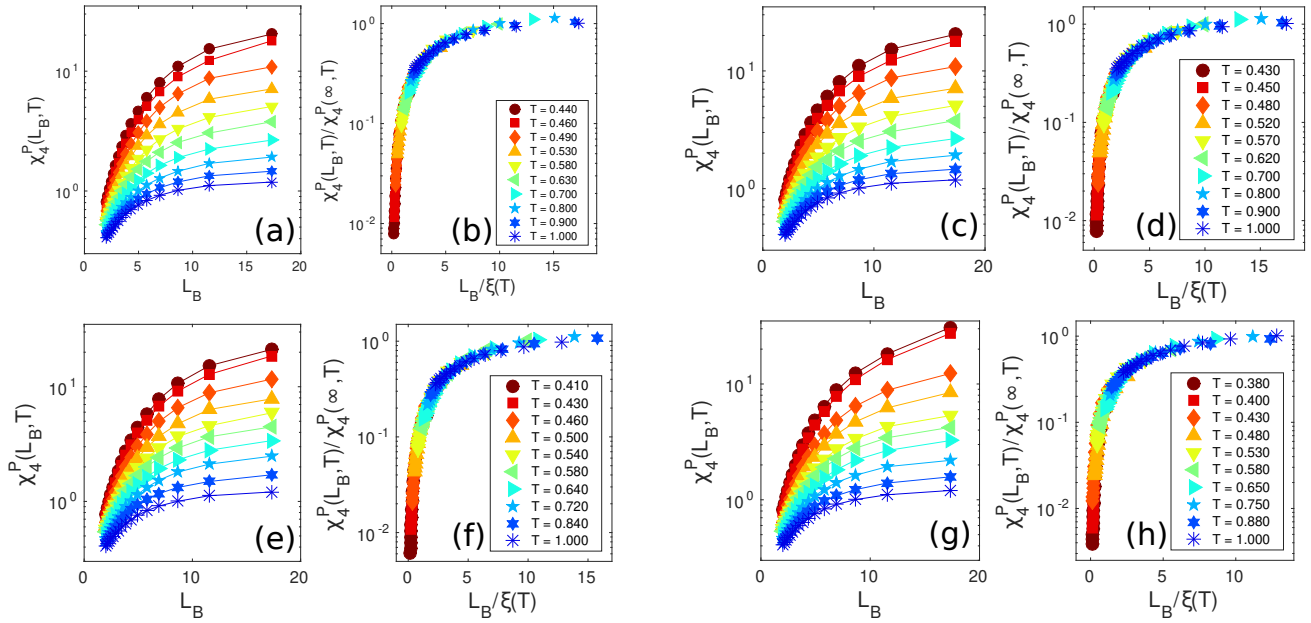

FIG. 1. Block size dependence of χ_4^P and finite size scaling for activity $f_0 = 0.5$ (a & b), $f_0 = 1.0$ (c & (d), $f_0 = 1.5$ (e & f), $f_0 = 2.0$ (g & h)

For each f_0, we consider the dependence of $\chi_4^P(L_B, T)$, the peak value of $\chi_4(L_B, t)$ at temperature T , on the block size L_B for a fixed value of $N = \rho L^3$. This dependence is shown in Fig.1 The left panel of each sub figure shows the data for $\chi_4^P(L_B, T)$ as a function of the block length L_B for different T. The peak value of the dynamical susceptibility at a given T grows with L_B and saturates at a T-dependent value $\chi_4^P(\infty, T)$. The dependence of $\chi_4^P(L_B, T)$ on L_B is expected to exhibit the following Finite Size Scaling (FSS) form:

$$\chi_4^P(L_B, T) = \chi_0(T) \mathcal{F}\left(\frac{L_B}{\xi}\right) \tag{5}$$

where,

$$\chi_0(T) = \lim_{L_B \to \infty} \chi_4^P(L_B, T) \tag{6}$$

and ξ is a characteristic scaling length scale. The data for all temperatures can be collapsed to a master curve using the two parameters, $\chi_4^P(\infty, T)$ and ξ, for each temperature, as shown in Fig. 1 for different activities. This length scale is found to be same as the the dynamic heterogeneity length scale, ξ_D as shown in [2] for the equilibrium system. The excellent data collapse confirms that the extracted length scales will be very reliable with small error bars (smaller than the point sizes in our plots).

B. Block analysis of van Hove function

The distribution of particle-displacements, known as the van Hove function, shows non-Gaussian behavior with exponential tail in the supercooled regime in glass-forming liquids. The non-Gaussian nature can be understood in terms of spatial and temporal heterogeneous dynamics and the exponential tail is a manifestation of dynamic heterogeneity. The van Hove correlation function is formally defined as

$$G_s(x,\tau) = \langle \delta[x - (x_i(\tau) - x_i(0))] \rangle, \tag{7}$$

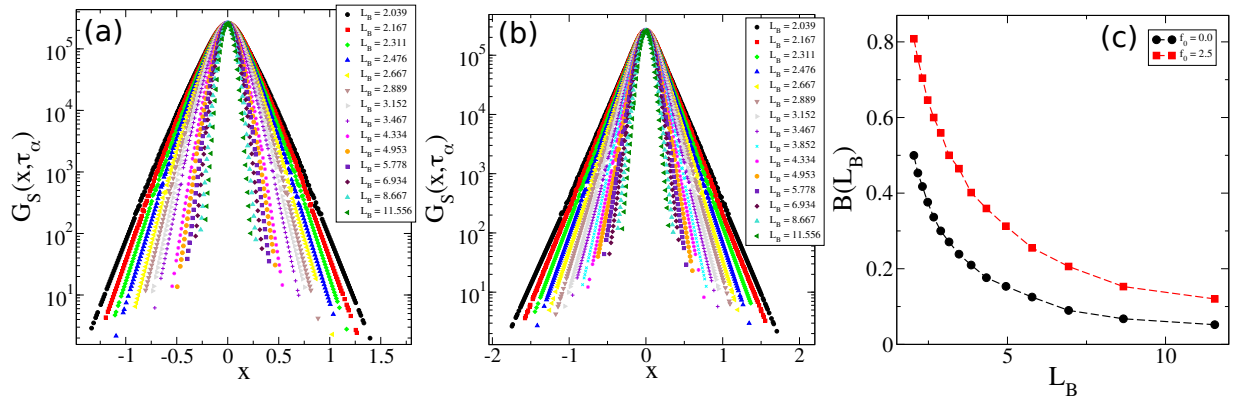

FIG. 2. The van Hove correlation function of different block lengths at lowest temperature for $f_0 = 0.0$ (a), $f_0 = 2.5$ (b), and corresponding Binder Cumulants (c).

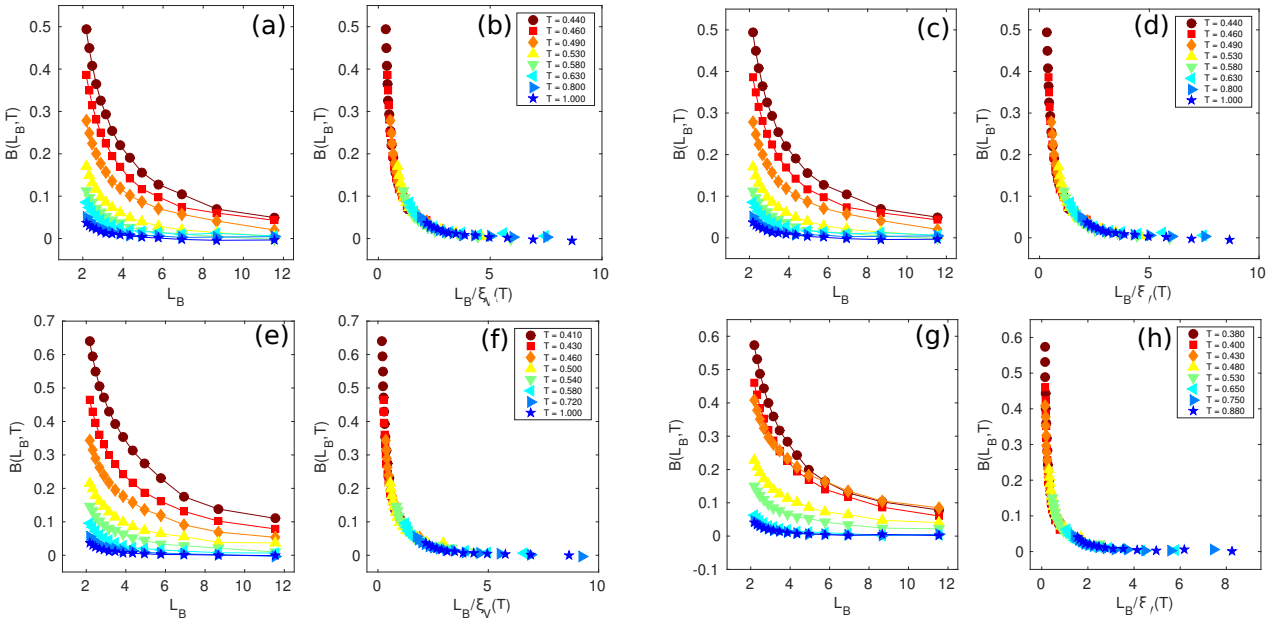

FIG. 3. Block size dependence of Binder Cumulant of Van-Hove function and finite size scaling for activity $f_0 = 0.5$ (a) and (b), $f_0 = 1.0$ (c) and (d), $f_0 = 1.5$ (e) and (f), $f_0 = 2.0$ (g) and (h).

where the $\langle \cdots \rangle$ implies the averaging over different statistically independent samples as well as the time origin averaging. We have performed systematic spatial coarse-graining of the dynamics to extract ξ_D of the system as demonstrated in [3]. To do that we have used the method of block analysis where the whole simulation box is divided into smaller blocks of length, L_B. Thus for a block size of L_B, the number of particles in that block will be $N_B = \rho L_B^3$.

Now we have defined a coarse-grained displacement of the particles in the j^{th} block as

$$\Delta x_j^B(\tau) = \frac{1}{n_j}\sum_{i=1}^{n_j}[x_i(\tau) - x_i(0)], \tag{8}$$

where n_j is the number of particles in the j^{th} block. Note that this number can be different for different blocks. Then we have defined the van Hove function for block as

$$G_s^B(x,\tau_\alpha) = \left\langle \frac{1}{N_B}\sum_{j=1}^{N_B}\delta[x - \Delta x_j^B(\tau_\alpha)] \right\rangle. \tag{9}$$

By increasing the block length L_B, we have then studied the non-Gaussianity for different block lengths. One can observe that the non-Gaussianity increases with decreasing block size in Fig. 2a (for $f_0 = 0.0$) and Fig. 2b (for $f_0 = 2.5$). To measure the non-Gaussianity, we have calculated the Binder Cumulant of the distribution, which is defined as

$$B(L_B,T) = 1 - \frac{\langle x^4\rangle}{3\langle x^2\rangle^2}. \tag{10}$$

To extract the temperature dependence of the coarse-graining length scale, we performed the finite-size scaling analysis of the Binder Cumulant with the following scaling function

$$B(L_B,T) = \mathcal{K}\left[\frac{L_B}{\xi_V(T)}\right]. \tag{11}$$

Note that this procedure removes the need to define any adhoc cut-off parameters to obtain the length scale. The scaling collapse looks quite good with the use of dynamic length scale ($\xi_V = \xi_D$) obtained in the block analysis method in the previous section. Hence we believe that the extracted length scale of the system ξ_D for all activities will be very reliable. The results are shown in Fig. 3. We also compared the Binder Cumulant of all block sizes in Fig. 2c for $f_0 = 0.0$ and $f_0 = 2.5$ where the τ_α of the both system is similar. This clearly show that the value of Binder Cumulant of van-Hove function and hence the associated length scale is bigger for active system than its passive counter part at similar structural relaxation timescale.

C. Displacement-displacement correlation function $\Gamma(r,\Delta t)$

To understand the physical mechanism behind the enhanced dynamic heterogeneity in the active glass-forming liquids, we have measured the spatial correlation in the displacement field of particles at $\Delta t = \tau_\alpha$. This was already shown in previous studies to correctly capture the temperature dependence of the dynamic heterogeneity length scale. In this work, we have also implemented the procedure given in [4, 5]. The spatial correlation of the particle displacements $g_{uu}(r,\Delta t)$ is defined as

$$g_{uu}(r,\Delta t) = \frac{\left\langle \sum_{i,j=1,j\neq i}^{N} u_i(t,\Delta t)u_j(t,\Delta t)\delta(r - \mid \mathbf{r}_{ij}(t) \mid)\right\rangle}{4\pi r^2 \Delta r N\rho \langle u(\Delta t)\rangle^2}, \tag{12}$$

where $u_i(t,\Delta t) = \mid \mathbf{r}_i(t+\Delta t) - \mathbf{r}_i(t) \mid$ is the scalar displacement of the particle between time t and $t+\Delta t$.

To extract the associated length scale we calculated the quantity called excess displacement-displacement correlation $\Gamma(r,\Delta t)$ defined as

$$\Gamma(r,\Delta t) = \frac{g_{uu}(r,\Delta t)}{g(r)} - 1, \tag{13}$$

where $g(r)$ is the radial pair correlation function given by

$$g(r) = \frac{1}{\rho N}\left\langle \sum_{i,j=1,j\neq i}^{N}\delta(\mathbf{r} + \mathbf{r}_i(0) - \mathbf{r}_j(0))\right\rangle. \tag{14}$$

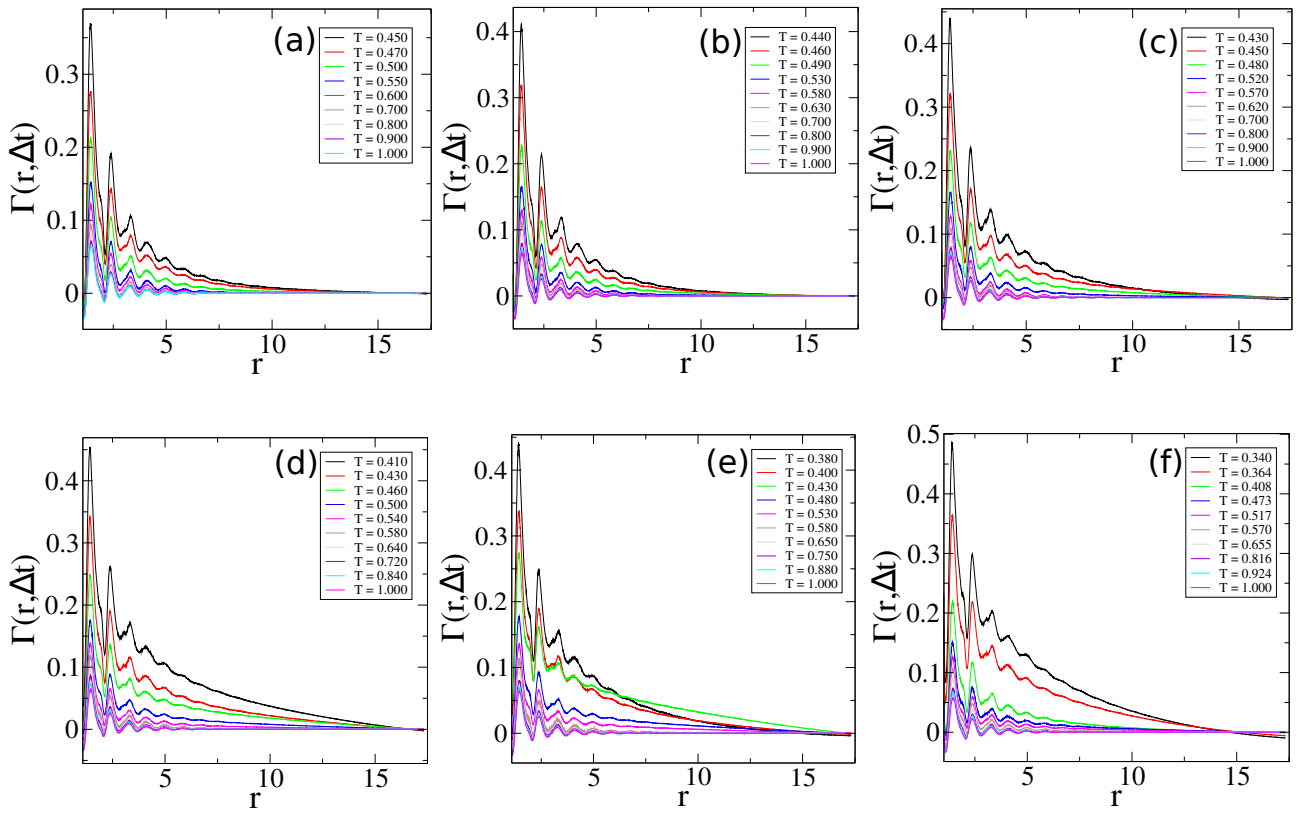

FIG. 4. excess displacement-displacement correlation $\Gamma(r, \Delta t)$ for all activities $f_0 = 0.0$ (a), 0.5 (b), 1.0 (c), 1.5 (d), 2.0 (e), 2.5 (f)

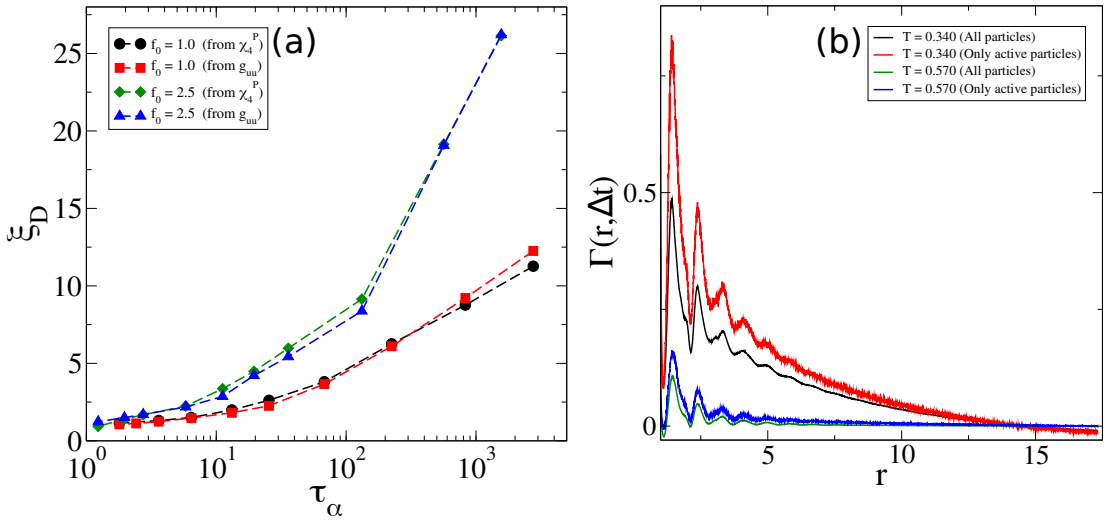

FIG. 5. (a) Comparison of ξ_D with two different methods for $f_0 = 0.0$ and $f_0 = 2.5$. (b) Excessive displacement-displacement correlation for full system and considering only active particles

With this definition the excess displacement-displacement correlation function goes to zero at large distance, $\lim_{r\to\infty} \Gamma(r, \Delta t) = 0$. We used $\Delta t = \tau_\alpha$ and calculated the excess displacement-displacement correlation $\Gamma(r, \Delta t)$

for all activities in Fig. 4. The integrated area gives the associated length scale. We also compared the length scale extracted from this method with the other two methods for $f_0 = 0.0$ and $f_0 = 0.0$ in Fig. 5. The extracted length scales from these different methods agree with each other very well. This also reconfirms the robustness of the methods used to compute the dynamic heterogeneity length scale in this study along with the reliability of the extracted length scale. Computation of length scale via different methods became necessity in this study as the results suggest a very dramatic rise in dynamic heterogeneity length scale with changing activity and we wanted to be completely sure that our observations are supported via all possible existing methods of measuring the dynamic heterogeneity length in the literature.

We have shown $\Gamma(r, \Delta t)$ for the highest activity $f_0 = 2.5$ at two different temperatures $T = 0.340$ ($\tau_\alpha = 1566.28$) and $T = 0.570$ ($\tau_\alpha = 11.195$) for $N = 50000$ in the right panel of Fig.5. We considered the full system as well as considering only the active particles. It is clear that the value of $\Gamma(r, \Delta t)$ is much higher if one considers only the active particles while computing the displacement-displacement correlation function rather than considering all the particles. This observation clearly tells that the active particles are probably setting up a longer range correlation in the system resulting in an enhanced dynamic heterogeneity. Understanding the origin of such longer range correlation with non-equilibrium active forcing will be an interesting future work and will be addressed elsewhere.

III. TEMPERATURE DEPENDENCE OF ξ_D

We present ξ_D as a function of $|\frac{T-T_K}{T_K}|$ for all activity in Fig. 6a where T_K is the 'Kauzmann temperature', the temperature at which the configuration entropy extrapolates to zero. We obtain T_K by fitting the $\tau_\alpha(T)$ data at different f_0 with the Vogel-Fulcher-Tammann equation: $\ln \tau_\alpha \sim 1/(T - T_K)$. There is a power law behaviour and we calculate the exponent ν_D for each f_0 using the relation $\xi_D(T) \propto \left|\frac{T-T_K}{T_K}\right|^{-\nu_D}$. Fig. 6b shows ν_D as a function of f_0. The exponent almost linearly increases with f_0.

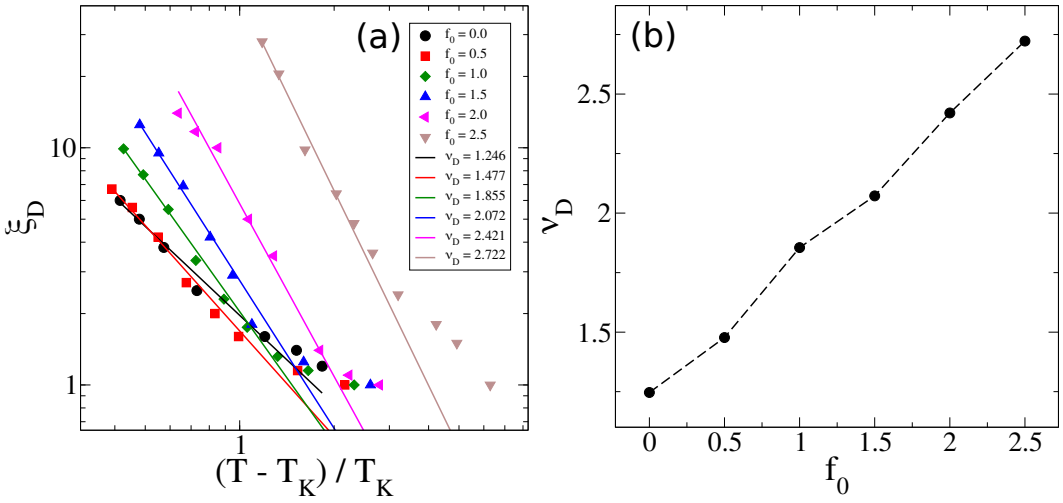

FIG. 6. (a) Dynamic heterogeneity length scale ξ_D as a function of $(T - T_K)/T_K$; lines are fits with the function $\xi_D \sim |(T - T_K)/T_K|^{\nu_D}$. (b) The exponent ν_D almost linearly increases with f_0.

Dependence of ξ_D with T_g/T

We have also presented the dynamic heterogeneity length scale, ξ_D, as a function of T_g/T in Fig. 7(b), where T_g is the calorimetric glass transition temperature, defined as $\tau_\alpha(T = T_g) = 10^6$. It clearly shows the dramatic increase of ξ_D with increasing f_0.

Figure 7(b) shows T_g as a function of f_0. From Eq. (1) in the main text, we find that MCT predicts $T_g = a - bf_0^2$ with a and b being two constants. Figure 7(b) shows that the simulation result agrees well with the MCT prediction.

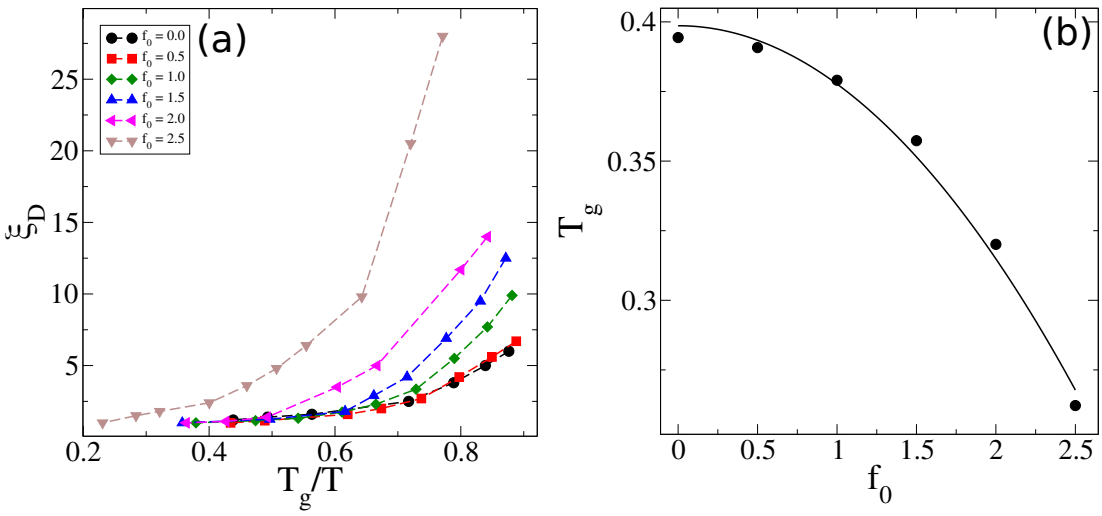

FIG. 7. (a) Dynamic heterogeneity length scale ξ_D as function of T_g/T to demonstrate the dramatic growth of length scale even when the relaxation nature of the system crosses over to strong liquid. This behaviour is strikingly different from equilibrium in which it is observed that dynamic heterogeneity gets suppressed for strong liquids. See text for details. (b) T_g as a function of f_0. Symbols are simulation data and the line is a fit with the MCT prediction $T_g = a - bf_0^2$ with $a \approx 0.40$ and $b \approx 0.02$.

IV. CORRELATION BETWEEN τ_α AND τ_{peak}

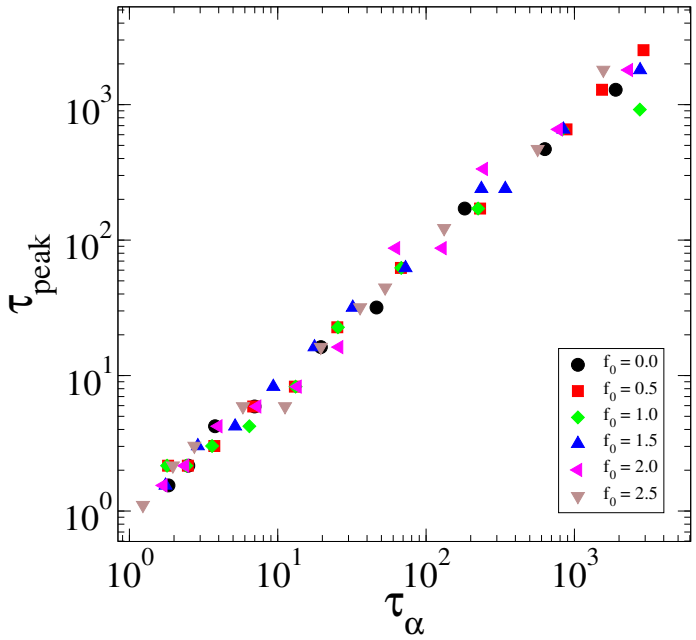

FIG. 8. The cross plot of τ_α and τ_{peak} for all the studied activity and temperature range. The nice data collapse confirms that the time at which the peak appears in $\chi_4(t)$ is proportional to the α-relaxation time of the system similar to the passive case.

The time, τ_{peak}, at which $\chi_4(t)$ attains its maximum gives a measure of relaxation time. Figure 8 shows τ_{peak} against τ_α, relaxation time obtained from $Q(t)$, of the system for all studied T and f_0. Near collapse of the data confirms that τ_{peak} is proportional to τ_α even in the presence of active forces. This observation, along with the analysis of τ_α presented in the main text, suggest that the relaxation dynamics, characterized via either $\chi_4(t)$ or $Q(t)$, can be understood by an effective-equilibrium-like description at an appropriate effective temperature.

V. COOPERATIVELY REARRANGING REGION (CRR)

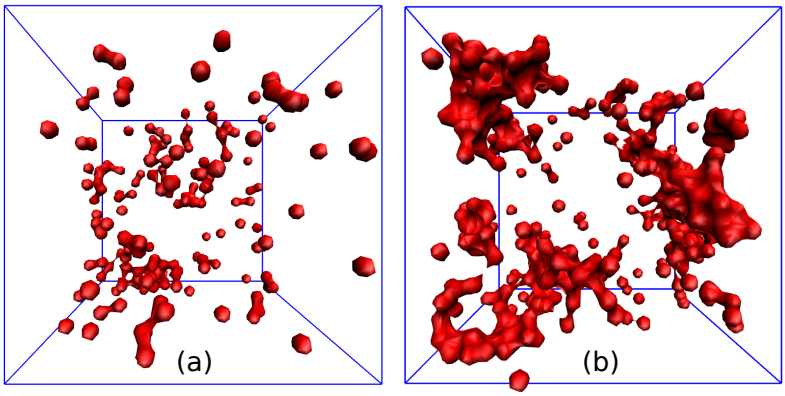

FIG. 9. clustering of faster particles at same τ_α for (a) $f_0 = 0.0$ and (b) $f_0 = 2.5$.

The dynamic heterogeneity scenario of glassy dynamics refers to the coexistence of dynamically slow and fast relaxing regions in the system. A region consisting of neighboring particles with comparable relaxation time relaxes collectively and known as cooperatively rearranging region (CRR). Thus, CRR provides a qualitative measure of dynamic heterogeneity in the system. To observe this region in three dimension, both for the passive and the active systems, we calculate the net displacement of each particles over a time-scale τ_α ($\sim 10^3$). We then consider only the faster particles whose displacements are greater than our chosen cut off value which is 9% of the whole simulation box. We plot the positions of these particles in the VMD software using the function "surf": each particle is represented by a small sphere of certain radius and if the distance between two particles are less than their diameter, they are collectively represented by a surface. Figure 9(a) shows a typical plot of the faster paricles for equilibrium glass while Fig. 9(b) shows the same for $f_0 = 2.5$; the parameters of the two systems are chosen such their τ_α are same. It is clear from the plot that unlike the equilibrium system, the CRR in case of active system is system spanning. This visualization gives a qualitative idea of enhanced dynamic heterogeneity in active glass compared to its equilibrium counterpart.

VI. RESULTS OF 3DHP

In this section, we present some of the main results obtained from 3dHP model system which confirm that the results presented in the main manuscript are generic and applicable to a wide class of model systems. Note that this model is very different from the 3dKA model which is a good model for molecular glass-forming liquids, whereas 3dHP is a paradigmatic model for soft sphere systems relevant for colloidal systems and has been widely studied in the context of jamming physics. The dynamic heterogeneity length scale ξ_D in this model is also computed in the same way as discussed before for 3dKA model. For a better comparison, we have used the same $\tau_p = 1.0$ in the simulations of the 3dHP model. The results are very similar as 3dKA model, presented in the main text. In Fig. 10 (a) we have shown the dynamic heterogeneity length scale ξ_D as a function of τ_α where the length scale at a particular τ_α is increasing with increasing f_0. In Fig. 10 (b) and (c) we have shown the overlap correlation function, $Q(t)$, and the four point susceptibility, $\chi_4(t)$. The parameters in these systems are chosen such that they all have similar τ_α, as confirmed from the plot fo $Q(t)$ [Fig. 10(b)]. It is clear that the peat height, χ_4^P, of $\chi_4(t)$ is monotonically increasing with increasing activity which has similar trend as 3dKA model. In Fig. 10 (d) and (e) we have shown ξ_D as function of T/T_K and $(T - T_C)/T_C$ respectively. There is a power law behaviour observed between ξ_D and the rescaled temperature as $\xi_D(T) \propto \left|\frac{T-T_C}{T_C}\right|^{-\gamma_D}$ with an exponent γ_D. The variation of this exponent γ_D is shown in the panel (f). γ_D seems to linearly increase with f_0, similar to the result in simulations of 3dKA model (Fig. 6).

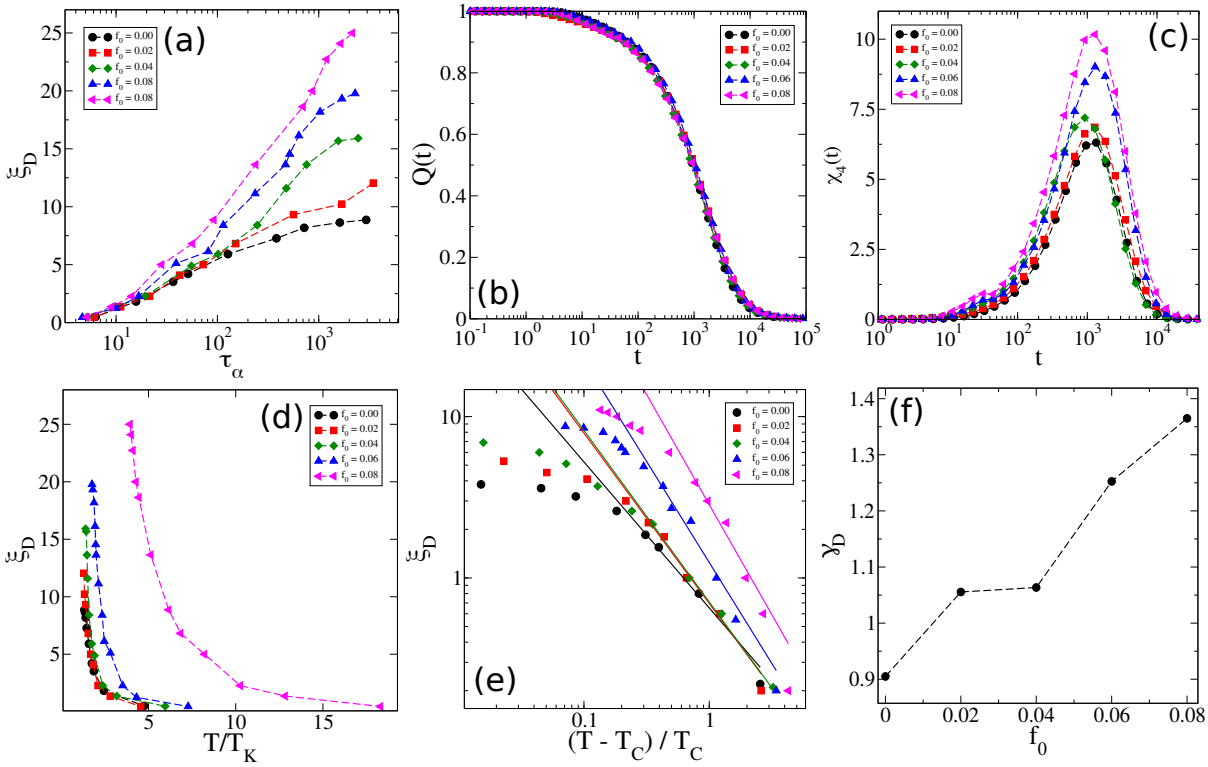

FIG. 10. Simulation results for the 3dHP model: (a) ξ_D as a function of τ_α for different f_0. (b) Overlap correlation function, $Q(t)$, for different activities where the systems have similar τ_α. (c) $\chi_4(t)$ for the same systems as in (b). (d) ξ_D as a function of T/T_K. (e) ξ_D as a function of $(T - T_C)/T_C$, lines are fits to the form $\xi_D \sim [(T - T_C)/T_C]^{-\gamma_D}$. (f) The exponent γ_D increases almost linearly with f_0.

[1] F. Zhang, J. Chem. Phys. **106**, 6102 (1997).
[2] S. Chakrabarty, I. Tah, S. Karmakar, and C. Dasgupta, Phys. Rev. Lett. **119**, 205502 (2017).
[3] B. P. Bhowmik, I. Tah, and S. Karmakar, Phys. Rev. E **98**, 022122 (2018).
[4] C. Donati, S. C. Glotzer, and P. H. Poole, Phys. Rev. Lett. **82**, 5064 (1999).
[5] W. Kob, C. Donati, S. J. Plimpton, P. H. Poole, and S. C. Glotzer, Phys. Rev. Lett. **79**, 2827 (1997).